CrossMark

Electromagnetic organ tracking allows for real-time compensation of tissue shift in image-guided laparoscopic rectal surgery: results of a phantom study

M. Wagner[1] · M. Gondan[2] · C. Zöllner[3] · J. J. Wünscher[1] · F. Nickel[1] ·
L. Albala[1] · A. Groch[3] · S. Suwelack[4] · S. Speidel[4] · L. Maier-Hein[3] ·
B. P. Müller-Stich[1] · H. G. Kenngott[1]

Abstract

Background Laparoscopic resection is a minimally invasive treatment option for rectal cancer but requires highly experienced surgeons. Computer-aided technologies could help to improve safety and efficiency by visualizing risk structures during the procedure. The prerequisite for such an image guidance system is reliable intraoperative information on iatrogenic tissue shift. This could be achieved by intraoperative imaging, which is rarely available. Thus, the aim of the present study was to develop and validate a method for real-time deformation compensation using preoperative imaging and intraoperative electromagnetic tracking (EMT) of the rectum.

Methods Three models were compared and evaluated for the compensation of tissue deformation. For model A, no compensation was performed. Model B moved the corresponding points rigidly to the motion of the EMT sensor. Model C used five nested linear regressions with increasing level of complexity to compute the deformation (C1–C5). For evaluation, 14 targets and an EMT organ sensor were fit into a silicone-molded rectum of the OpenHELP phantom. Following a computed tomography, the image guidance was initiated and the rectum was deformed in the same way as during surgery in a total of 14 experimental runs. The target registration error (TRE) was measured for all targets in different positions of the rectum.

Results The mean TRE without correction (model A) was 32.8 ± 20.8 mm, with only 19.6 % of the measurements below 10 mm (80.4 % above 10 mm). With correction, the mean TRE could be reduced using the rigid correction (model B) to 6.8 ± 4.8 mm with 78.7 % of the measurements being <10 mm. Using the most complex linear regression correction (model C5), the error could be reduced to 2.9 ± 1.4 mm with 99.8 % being below 10 mm.

Conclusion In laparoscopic rectal surgery, the combination of electromagnetic organ tracking and preoperative imaging is a promising approach to compensating for intraoperative tissue shift in real-time.

Keywords Rectal cancer · Laparoscopy · Image-guided surgery · Motion compensation

✉ H. G. Kenngott
hannes.kenngott@med.uni-heidelberg.de

[1] Department of Surgery, Heidelberg University Hospital, Im Neuenheimer Feld 110, 69120 Heidelberg, Germany

[2] Department of Psychology, University of Copenhagen, Copenhagen, Denmark

[3] Junior Group Computer-Assisted Interventions, German Cancer Research Center, Heidelberg, Germany

[4] Institute for Anthropomatics and Robotics, Karlsruhe Institute of Technology, Karlsruhe, Germany

Laparoscopic colorectal surgery has a steep learning curve, and a high level of experience is necessary to prevent complications and to provide oncologic safety [1]. Computer-based image guidance could allow for visualization of risk and target structures and may help to identify the correct resection area to optimize intraoperative as well as postoperative outcome.

Image-guided surgery is widely used in neurosurgery, orthopedics and ear–nose–throat surgery [2–4], but remains, however, of limited use in laparoscopic surgery. This is largely attributed to the organ shift caused by respiration, heartbeat, as well as tissue deformation by surgical

🖄 Springer

manipulation [5–7]. Intraoperative imaging capable of assessing these different types of motion is rarely available because it is expensive and not easily integrated into the surgical workflow [8]. Therefore, we decided to track the motion of the organ with an attached sensor.

The aim of the present study was to develop a method that is able to detect organ motion and deformation via intraoperative electromagnetic tracking (EMT) so that there is no need for intraoperative imaging. In addition, the robustness of this method, its limitations and directions for future work and clinical application were evaluated.

Materials and methods

Method for compensation of motion and deformation

Different models were employed to calculate the intraoperative motion and deformation of the rectum by deploying real-time information obtained from an EMT-based organ sensor. Therefore, we treated the rectum as a flexible tube, which was fixed at the pelvic floor and mobile at the rectosigmoidal junction, where it was pulled (Figs. 1, 2).

For model A, the information from the EMT was not used. Thus, no compensation was performed and image

guidance information was based only on preoperative imaging data. For model B, the motion of the targets along the rectum was assumed to follow the motion vector of the EMT sensor, e.g., to have the same length and orientation. This compensated for the motion but not for deformation of the rectum. For model C, five nested linear regression models with increasing level of complexity (C1–C5, Table 1; Supplement 1) were tested to find out whether the deformation of the rectum could be computed from the motion of the electromagnetic sensor based on linear regression.

To achieve this, the Heidelberg Minimally Invasive Navigation Device (HD-MIND, former use for minimally invasive esophagectomy described in [9]) was programmed using the Medical Imaging Interaction Toolkit (MITK) [10]. The new version of the image guidance system, which is described in the present study, allowed for simultaneous use of an optical and an EMT system to combine precision and wireless convenience of optical tracking for the laparoscopic instruments with EMTs capability for an organ (motion) sensor.

Experimental setup

The experiments were performed using the pelvic module of the Heidelberg Laparoscopy Phantom (OpenHELP)

Fig. 1 **A** Rectal organ made of silicone with fourteen glass targets in perpendicular order and the organ sensor, an electromagnetically tracked catheter in the crossing. Targets 1–5 are counted from the bottom-up to below the *horizontal line*. Targets 6–10 are the *horizontal line* from left to right, and targets 11–15 are continuously counted above the *horizontal line*. **B** Virtual representation within the pelvic phantom after CT imaging
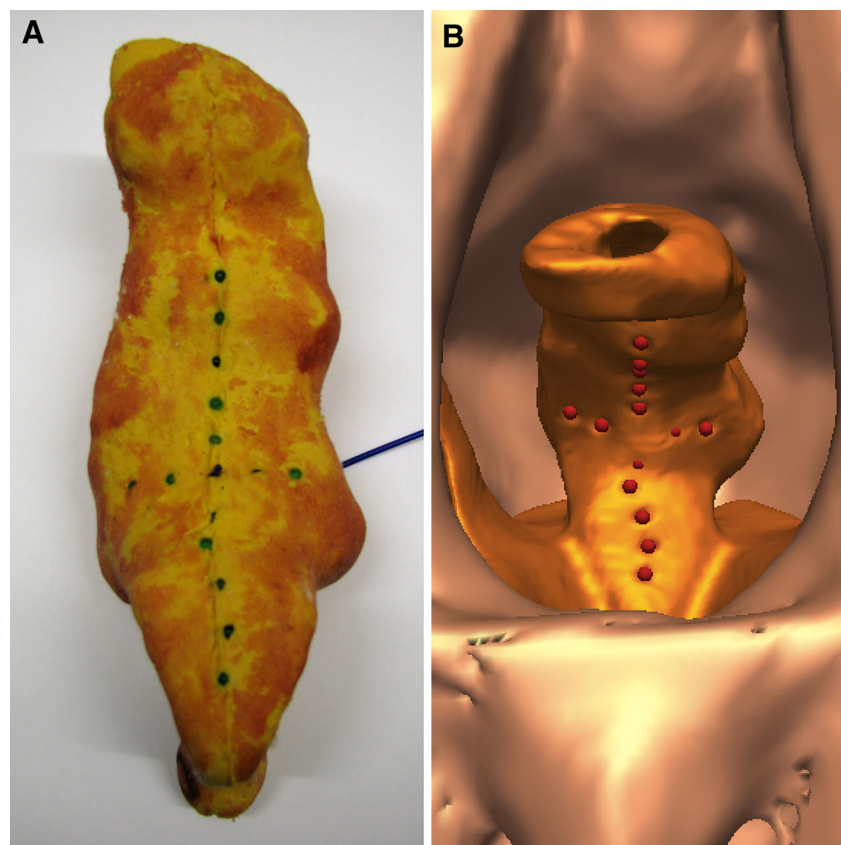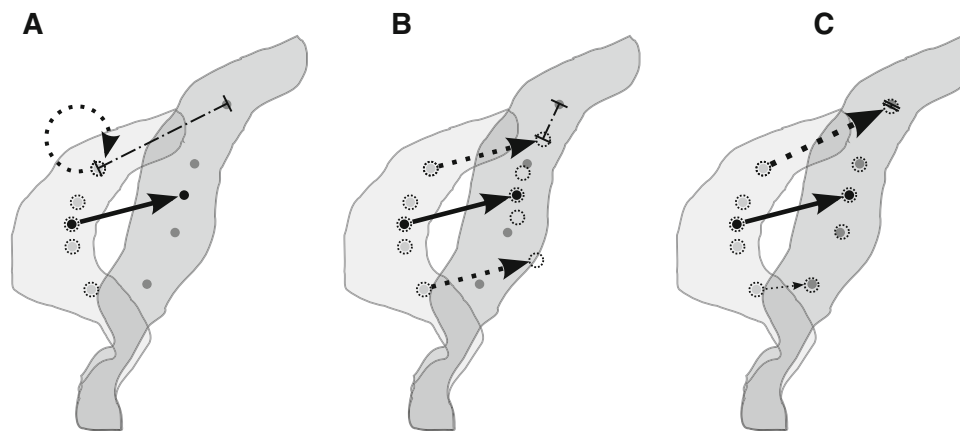
Fig. 2 Schematic visualization of the different correction models with the rectum in initial position (*light gray*) and stretched (*dark gray*). The visualization shows correction model A (**A**), B (**B**) and C5 (**C**). For further details on the models C1–C4, see Supplement 1. The *gray dots* represent the glass targets, whereas the *black dot* represents the position of the sensor. The *black arrows* show the motion of the sensor; from this, the motion of the targets is calculated (*dotted arrows*). The calculated position is marked with *dotted circles* that match the initial position, but not the real position (model A), roughly match the real position for some targets near the sensor (model B) or almost completely match the real position (model C5). Accordingly, the target registration error (TRE, *dot-dashed line*) decreases from model A to C

Table 1 Summary of the different models to compensate for motion and deformation

Model	Compensation of motion and deformation	Explanation
A	No compensation	
B	Rigid motion compensation	The targets are moved exactly as the organ sensor was moved
C1	Compensation of elongation of the organ	Stepwise scaling of sensor motion according to target position in relation to the sensor
C2	Linear compensation of elongation of the organ	Same as C1 but with scaling factor based on linear regression on sensor height
C3	Compensation of elongation and motion	Same as C2 but with an additional constant to correct for motion of the whole organ
C4	Compensation of deformation and motion	Same as C3, but with additional quadratic regression based on sensor position to account for bending of the organ
C5	Target-specific compensation	Regression on single targets. The organ was considered as a collection of independent single elements.

[11]. The OpenHELP was based on segmentation of organs from a computed tomography (CT) scan of a young man, and the elements were fabricated using rapid prototyping. The pelvic module consisted of a plaster-based male pelvis, as well as a rectum (including mesorectum) and muscles of the pelvic floor, which were fabricated of silicone. The connective tissue surrounding the rectum was reconstructed from soft cotton. The whole phantom was immobilized on a vacuum mattress according to the method already established in HD-MIND for minimally invasive esophagectomy [9].

The organ sensor was placed in the wall of the rectum (see "EMT and organ tracking" section). Fourteen glass targets with a diameter of 3 mm were attached to the outer wall of the silicone organ to evaluate the accuracy of the motion compensation in different parts of the organ (Fig. 1). Targets 1–5 were placed above the sensor, and targets 11–15 were placed below the sensor. Targets 6–10 were placed at the level of the sensor: targets 6 and 7 to the left, targets 9 and 10 to the right of the sensor. The sensor was target 8. The distance between two adjacent targets was 5 mm.

Six registration fiducials were attached to the pelvic surface (Fig. 3). Each registration fiducial had a defined center that was visible in the CT image and could precisely be targeted with a tracked pointing device in order to register the phantom to the acquired images.

EMT and organ tracking

EMT is the method of choice when accurate tracking is needed, but no direct line of sight toward the target is available. Therefore, it was chosen for organ tracking in this study, even if it holds some limitations such as wires to

the sensors and susceptibility to distortion in ferromagnetic environments as Franz et al. [12] discuss in a conclusive review of EMT technology and its application in medicine.

The Aurora®-System (Northern Digital Inc., Waterloo, Canada) was used. It comprises a field generator, a reference sensor and an organ sensor. The planar field generator (version 1) was fixed next to the field of interest that was aligned with the EMT's tracking volume of $500 \times 500 \times 500$ mm as stated by the manufacturer. Whereas previous studies showed that the specified tracking volume of $500 \times 500 \times 500$ mm can be achieved, the tracking volume should be limited to about $190 \times 190 \times 190$ mm to achieve reasonable accuracy in an operating-room (OR) setting [13]. Furthermore, in this study, we positioned the whole setup on a metal-free table to eliminate tracking errors caused by ferromagnetic field distortions. The reference sensor (Aurora® reference body with six degrees of freedom) was positioned between the pelvic phantom and the vacuum mattress. The organ sensor was a catheter wire of the EMT system with five degrees of freedom. It was inserted into the wall of the silicone rectum and fixed by the adhesive properties of the material (Fig. 1A).

Additionally, porcine experiments for endoluminal sensor fixations were undertaken to prove feasibility of the approach, in this case for esophageal surgery (Fig. 4). Here, the tip of the sensor was wrapped with Leukosilk® tape that was fixed to hemoclips (Endotherapy Short Clip HX-610-090S; Olympus Medical, Tokyo, Japan). These clips were then attached to the organ mucosa using a flexible double-channel video endoscopy (PKS 13806 and Gastro Pack; Karl Storz Endoscopy, Tuttlingen, Germany). This animal study was approved by the German Committee on Animal Care, Regierungspräsidium Karlsruhe.

Image guidance experiment

The whole experimental run was performed 14 times. After CT scanning of the phantom with a slice thickness of 1 mm, the imaging data were loaded into the image guidance system. The tip of the EMT organ sensor, the glass targets and each center of the registration fiducials were marked in the images. Then, both tracking systems were aligned with the imaging data and the phantom using point-based registration with the algorithm of Horn [14]. This was performed using both an EMT and an optically tracked pointer, for each of the six registration fiducials. The fiducial registration errors (FRE) for both systems were assessed for each experimental run. Then mean and standard deviations were calculated for each FRE, respectively.

The rectum was subsequently mobilized using laparoscopic instruments. For each experimental run, ten different deformations with increasing stretch were simulated, resulting in a continuous deformation pattern from no pull to strong pull (Fig. 3). Simultaneously, the motion of the EMT organ sensor, e.g., the difference vector between the current position and the initial position, was measured to calculate the deformation based on real-time information

Fig. 3 Pelvic module of the OpenHELP phantom with six registration fiducials (black). Different extents of rectal mobilization are shown: A rectum immobilized in cotton wool, B rectum mobilized but not pulled, C medium pull on rectum, D strong pull
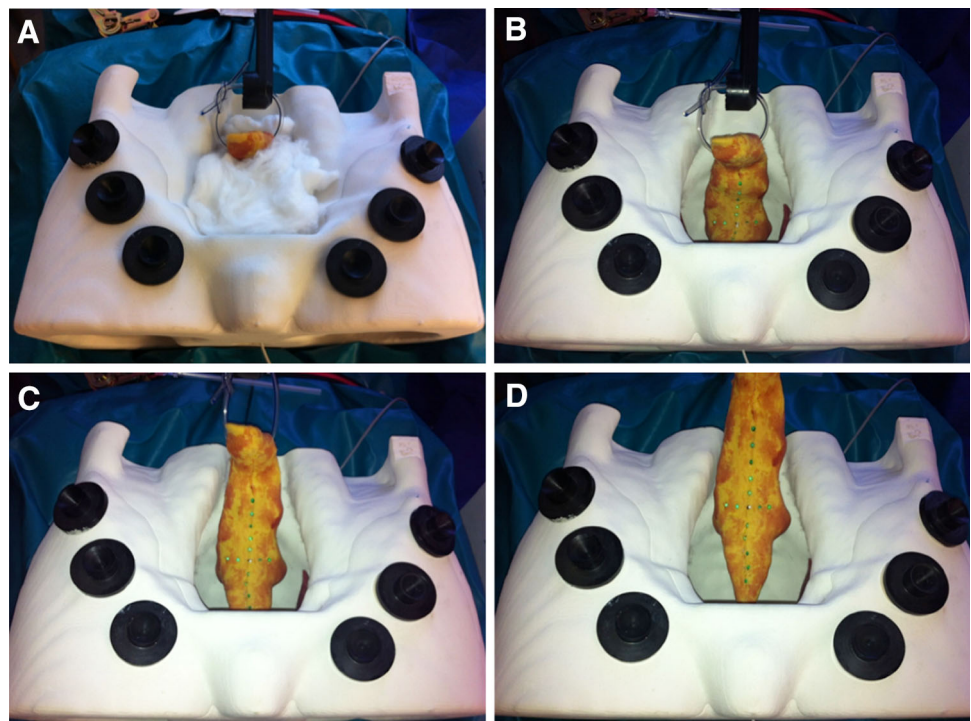
Fig. 4 Electromagnetic organ sensor is wrapped with Leukosilk® tape that forms a loop at the end and can be handled with a gastrocscope (**A**). This loop is then used to fix the sensor to luminal wall of the organ (here esophagus) with a hemoclip (**B**)
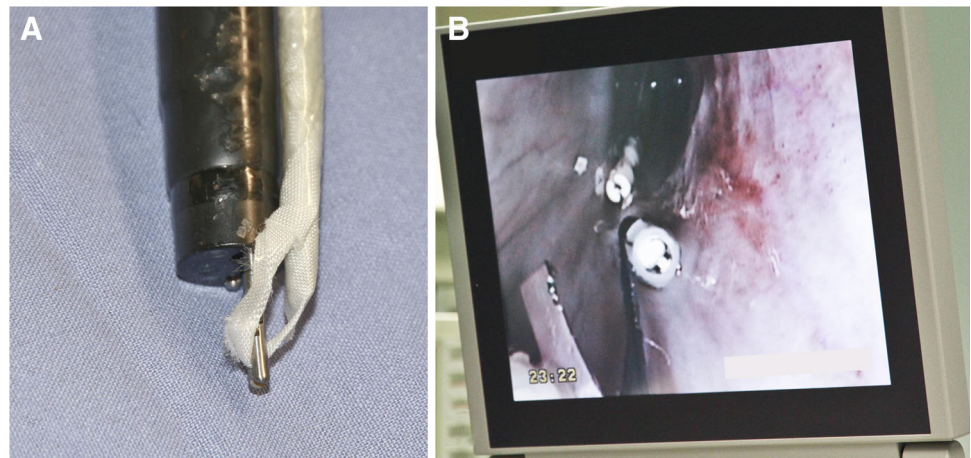
(Fig. 2). This difference vector represents the motion of the rectum. To obtain ground truth for evaluating the precision of the proposed method, the positions of the 15 targets (14 glass targets and the EMT sensor as target 8) were measured with the optically tracked pointer.

The target registration error (TRE) of all fifteen targets was calculated for each deformation step as the distance between the real-world position of a target and its virtual position in the image guidance system, which was possible because with the previous registration procedure the coordinate spaces were aligned (Fig. 2).

Statistical analysis

The results were preprocessed and analyzed using the software R [15]. Mean and standard deviation of the TRE were calculated for the acquired measurements. Furthermore, the proportion of TREs below 10 mm was calculated to introduce an additional metric for the systems safety. This value was chosen after discussion with surgical experts who demanded this to be the maximum error acceptable to rely on an image guidance system in their intraoperative decision making. The results of models A and B were tested against each other with Student's t test. Analysis of variance (ANOVA) was used to test the difference between models C1–C5 with nested complexity.

Results

The average FRE was 0.5 mm (SD 0.1 mm) for the optical tracking system and 0.7 mm (SD 0.3 mm) for the EMT system.

TRE of the different models

The average TRE without any correction (model A) was 32.8 mm (SD 20.8 mm) with only 19.6 % of the measurements below 10 mm. For the rigid motion compensation (model B), the average TRE was 6.8 mm (SD 4.8 mm) with 78.7 % of the measurements below 10 mm. Student's t test revealed a statistically significant difference between the TREs obtained by models A and B ($p < 0.001$). For the different levels of complexity of model C, the average TRE ranged from 2.9 mm (SD 1.4 mm) with 99.8 % below 10 mm for the model with highest complexity (C5, target-specific linear regression) to 10.3 mm (SD 8.8 mm) with 63.9 % below 10 mm for the level with lowest complexity (C1, unspecific scaling factor). ANOVA showed that each successive more complex level was significantly better than the previous one. However, only C5 was significantly better than the rigid correction of model B (Table 2).

TRE of the different targets

A closer examination of models A and B reveals different results for the different targets. Whereas model B has only 78.7 % of measurements of TRE below 10 mm for all targets, eight targets had more than 98 % of measurements of TRE below 10 mm. Figure 5 shows the results for models A and B for three target subgroups: targets 1–5 (above the sensor), targets 6–10 (at the level of the sensor) and targets 11–15 (below the sensor).

Discussion

Compensation model

Our system showed the feasibility of preoperative imaging in combination with EMT for compensation of intraoperative tissue deformation and the benefit of using different correction models in rectal surgery in a phantom model.

The corrected TRE (model B and C), calculated using the information from the EMT organ sensor, was

Table 2 Results for the different correction models

Model	Mean TRE	SD	% below 10 mm	Parameters
A	32.8	20.8	19.6	0
B	6.8	4.8	78.7	0
C1	10.3	8.8	63.9	0
C2	9.4	7.1	65.4	3
C3	8.4	5.2	69.6	6
C4	7.3	5.1	75.3	9
C5	2.9	1.4	99.8	33

Mean, standard deviation (SD) and proportion of TREs below 10 mm. The number of parameters in the respective model is a measure for its complexity. Detailed mathematical equations of the linear regression models can be found in Supplement 1

significantly lower than the uncorrected TRE (model A). Since the results varied between the different targets and calculation models, the necessity for a deformation model for rectal surgery became evident. For the targets at the level of the sensor, more than 98 % of the measured TRE were below 10 mm. The other targets varied more depending on the motion of the organ. For the targets below the sensor, there was an inverse dependence of corrected (model B) and uncorrected (model A) TRE on organ motion. This was due to the fact that the rectum was fixed to the pelvic floor at its bottom, which is not respected by model B. This led to an overcompensation of the TRE with model B; overcompensation was higher, the less the target itself moved.

Thus, model C was used taking the deformation of the organ into account. The results show that only the most complex model C5, employing separately calculated parameters for each of the target points, allowed for more accurate tracking of the whole organ than model B. This may be due to the fact that models C1–C4 applied a linear regression calculated for all of the targets, thus limiting the accuracy to an intermediate level even in high proximity to the sensor. Here,

model B already showed good results for the targets 3–11 arranged with five of the targets at the level of the sensor, two targets above and one target below the sensor (Fig. 5).

Thus, it can be questioned whether the increased complexity of model C is at all necessary: If the sensor can be placed in the vicinity of the targeted tumor and planned resection area, the rigid correction of model B could be sufficient. Furthermore, model C would be difficult to translate into clinical application: In order to calculate regression for the deformation model, the deformation would have to be examined beforehand or additional markers (represented by glass targets in this study) have to be introduced which would disturb the clinical workflow.

In summary, the system allowed for real-time tracking of the rectum with a high accuracy in the vicinity of the sensor (Fig. 5B shows targets at level of the sensor). Thus, the system could help less experienced surgeons to identify the oncologically correct height of resection in rectal cancer resection. This is especially relevant for patients who experienced previous surgeries as the operation is here more challenging due to scarring and iatrogenic changes in anatomy. Moreover, in the setting of recurrent cancer or reoperation for complications, the site lacks anatomical features that help the surgeon to navigate. The same is true for difficult operations such as morbidly obese patients or locally advanced tumors. In this case, even experienced surgeons could benefit from image guidance.

Deformation compensation in the literature

Most of the standard approaches to accounting for organ deformation, such as in liver surgery, are not suitable for application in rectal surgery. They consist of surface reconstruction followed by either rigid or non-rigid registration to tomographic images [16, 17]. The rectum, however, has no well-defined surface as the liver does, and its appearance is largely influenced by surgical manipulation.
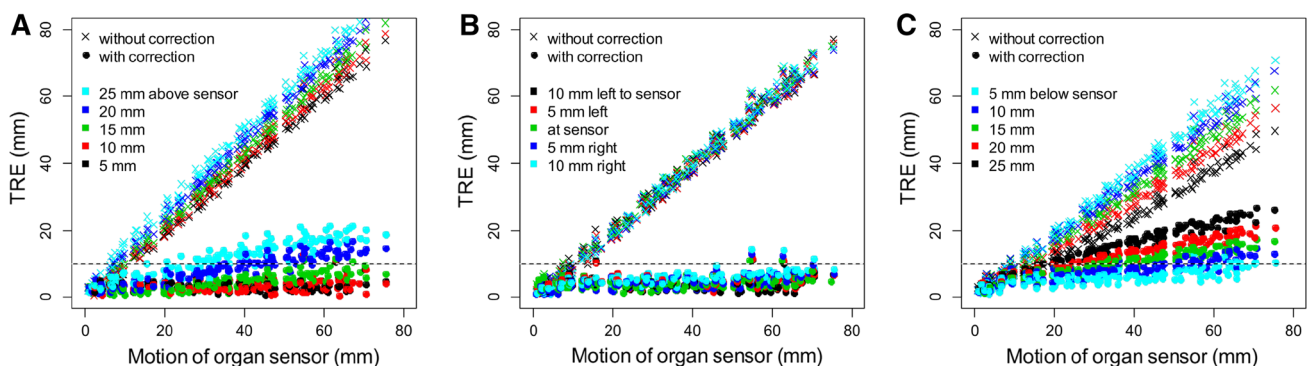
Fig. 5 Comparison of models A (*crosses*—without correction) and B (*dots*—with correction). TRE in mm (*y axis*) depending on the motion of the organ sensor in millimeter (*x axis*). The results are stratified by their position in relation to the organ sensor with the distance to the sensor color-coded: **A** targets above the sensor (targets 1–5), **B** at the level of the sensor (targets 6–10) and **C** below the sensor (targets 11–15)

Furthermore, the rectum as well as the colon resembles a flexible tube and lacks the geometric characteristics that are crucial for surface-based registration [18]. This implies that real-time information from surface reconstruction is unlikely to achieve accurate monitoring of motion and deformation in these organs. Intraoperative imaging that would allow for three-dimensional measurement of the deformation is mostly lacking and not easily integrated into the surgical workflow [8].

Hybrid tracking solutions, namely a combination of optical and EMT, were employed by different groups [19–21]. While hybrid tracking is usually intended to address the line-of-sight problem of optical tracking without losing its superior accuracy compared to the EMT, our approach was direct electromagnetic tracking of the target organ. Previous work used either superficial [22] or inserted markers [23–25] for organ tracking in image-guided surgery and intervention. Beller et al. [25] placed an EMT sensor next to a hepatic tumor and defined a "no-contact" area around it. When the optically tracked instrument entered this region, the surgeon was warned acoustically. This tracked area was, however, rigidly fixed to the EMT sensor and did not employ a deformation model.

Rassweiler et al. [26] proposed a marker-based approach of rigid organ tracking named inside-out tracking. For tracking, they used intraoperatively positioned surface markers in the laparoscopy video and provided an augmented reality based on intraoperative ultrasound imaging. In rectal surgery, however, the positioning of the markers could lead to injury of the mesorectal plane and therefore compromise oncological outcome [27]. Furthermore, due to the circular dissection of the mesorectal plane, the markers would not be visible most of the time. Thus, a marker-based technique is not applicable.

Shekhar et al. [28] did not use a tracking system at all. They facilitated organ tracking via continuous intraoperative CT imaging, but at the same time causing extensive radiation exposure to both the patient and the surgeon. Nevertheless, integration of CT imaging into the OR was already shown to be feasible in laparoscopic surgery and, in theory, is an alternative to our approach [8].

Clinical translation

The main limitation of the present study is that it is not clear whether the results of this phantom experiment are also applicable in a more realistic setting due to different tissue properties or inferior tracking conditions for both optical and EMT.

Firstly, the anchoring of the sensor and finding landmarks for evaluation of the system is certainly more difficult in real tissue. Thus, we conducted porcine experiments on the esophagus, where attaching the sensor to the mucosa proved feasible (Fig. 5). Despite differences in the organ anatomy from a surgical perspective, this method could easily be transferred to the rectum. Furthermore, laparoscopic clips should replace the glass targets used in this study. They can be securely fixed to the organ, targeted during the experiment itself, and their position can be determined in CT imaging to allow for calculation of image guidance errors as proved in previous studies [29].

Secondly, the clinical environment can compromise the accuracy of EMT. A metal OR table can cause serious distortions to the magnetic field, thus leading to higher tracking errors compromising the overall accuracy of the system. In extreme cases, this might render the whole image guidance system useless because of errors that can be as high as several centimeters. With conventional field generators, this problem can only be addressed by elevating the tracking volume from the table [13]. In clinical reality, this could be achieved using a vacuum mattress that would secure the patient on the table in case of Trendelenburg positioning during the pelvic part of the operation. Also new flat panel field generators have been developed which shield the tracking volume from distortions and could be positioned directly beneath the patient. Using this technology, Maier-Hein et al. [30] reduced the error resulting from the table in a CT suite setting by up to 70 % compared to the field generator used in our study.

Thirdly, the pointer used for evaluation was tracked optically in this study. In a clinical setting, optical instrument tracking could cause problems due to an interrupted line of sight. EMT for instrument tracking on the other hand would mean additional wires being attached to the laparoscopic instruments, which is inconvenient. Thus, we designed a laparoscopic instrument with improved optical tracking capabilities. It has already been tested in porcine studies without organ tracking, reduced the line-of-sight problem and allowed for precise evaluation of the image guidance system [29].

Still, application in animal experiments and subsequently clinical settings is necessary to evaluate the system in vivo. Here, the further development of the concept of EMT organ tracking for image-guided rectal cancer surgery is also determined by its integration into the clinical workflow.

Conclusion

The presented method for organ tracking allows for compensation of rectal motion and deformation for image-guided laparoscopic colorectal surgery in a phantom model. In the future, motion-compensated image guidance might help to lower the complexity of challenging

minimally invasive operations, especially for the less experienced surgeons. On the other hand, experienced surgeons might use this technology in difficult cases, for instance with morbidly obese patients, locally advanced or recurrent tumors.

References

1. Jamali FR, Soweid AM, Dimassi H, Bailey C, Leroy J, Marescaux J (2008) Evaluating the degree of difficulty of laparoscopic colorectal surgery. Arch Surg 143:762–767. doi:10.1001/archsurg.143.8.762

2. Schulz C, Waldeck S, Mauer UM (2012) Intraoperative image guidance in neurosurgery: development, current indications, and future trends. Radiol Res Pract. doi:10.1155/2012/197364

3. Justice JM, Orlandi RR (2012) An update on attitudes and use of image-guided surgery. Int Forum Allergy Rhinol 2:155–159. doi:10.1002/alr.20107

4. Hetaimish BM, Khan MM, Simunovic N, Al-Harbi HH, Bhandari M, Zalzal PK (2012) Meta-analysis of navigation vs conventional total knee arthroplasty. J Arthroplasty 27:1177–1182. doi:10.1016/j.arth.2011.12.028

5. Clifford MA, Banovac F, Levy E, Cleary K (2002) Assessment of hepatic motion secondary to respiration for computer assisted interventions. Comput Aided Surg 7:291–299. doi:10.1002/igs.10049

6. Wysocka B, Kassam Z, Lockwood G, Brierley J, Dawson LA, Buckley CA, Jaffray D, Cummings B, Kim J, Wong R, Ringash J (2010) Interfraction and respiratory organ motion during conformal radiotherapy in gastric cancer. Int J Radiat Oncol Biol Phys 77:53–59. doi:10.1016/j.ijrobp.2009.04.046

7. Zijlmans M, Langø T, Hofstad EF, Van Swol CFP, Rethy A (2012) Navigated laparoscopy–liver shift and deformation due to pneumoperitoneum in an animal model. Minim Invasive Ther Allied Technol 21:241–248. doi:10.3109/13645706.2012.665805

8. Kenngott HG, Wagner M, Gondan M, Nickel F, Nolden M, Fetzer A, Weitz J, Fischer L, Speidel S, Meinzer H-P, Böckler D, Büchler MW, Müller-Stich BP (2014) Real-time image guidance in laparoscopic liver surgery: first clinical experience with a guidance system based on intraoperative CT imaging. Surg Endosc 28:933–940. doi:10.1007/s00464-013-3249-0

9. Kenngott HG, Neuhaus J, Müller-Stich BP, Wolf I, Vetter M, Meinzer H-P, Köninger J, Büchler MW, Gutt CN (2008) Development of a navigation system for minimally invasive esophagectomy. Surg Endosc 22:1858–1865. doi:10.1007/s00464-007-9723-9

10. Nolden M, Zelzer S, Seitel A, Wald D, Müller M, Franz AM, Maleike D, Fangerau M, Baumhauer M, Maier-Hein L, Maier-Hein KH, Meinzer H-P, Wolf I (2013) The Medical Imaging Interaction Toolkit: challenges and advances : 10 years of open-source development. Int J Comput Assist Radiol Surg 8:607–620. doi:10.1007/s11548-013-0840-8

11. Kenngott HG, Wünscher JJ, Wagner M, Preukschas A, Wekerle AL, Neher P, Suwelack S, Speidel S, Nickel F, Oladokun D, Maier-Hein L, Dillmann R, Meinzer HP, Müller-Stich BP (2015) OpenHELP (Heidelberg laparoscopy phantom): development of an open-source surgical evaluation and training tool. Surg Endosc. doi:10.1007/s00464-015-4094-0

12. Franz AM, Haidegger T, Birkfellner W, Cleary K, Peters TM, Maier-Hein L (2014) Electromagnetic tracking in medicine—a review of technology, validation, and applications. IEEE Trans Med Imaging 33:1702–1725. doi:10.1109/TMI.2014.2321777

13. Kenngott HG, Wegner I, Neuhaus J, Nickel F, Fischer L, Gehrig T, Meinzer HP, Müller-Stich BP (2013) Magnetic tracking in the operation room using the da Vinci(®) telemanipulator is feasible. J Robot Surg 7:59–64. doi:10.1007/s11701-012-0347-2

14. Horn BKP, Hilden HM, Negahdaripour S (1988) Closed-form solution of absolute orientation using orthonormal matrices. J Opt Soc Am A 5:1127–1135. doi:10.1364/JOSAA.5.001127

15. R Core Team (2012) R: A Language and Environment for Statistical Computing. R Foundation for Statistical Computing, Vienna

16. Peterhans M, Oliveira T, Banz V, Candinas D, Weber S (2012) Computer-assisted liver surgery: clinical applications and technological trends. Crit Rev Biomed Eng 40:199–220

17. Nicolau S, Soler L, Mutter D, Marescaux J (2011) Augmented reality in laparoscopic surgical oncology. Surg Oncol 20:189–201. doi:10.1016/j.suronc.2011.07.002

18. Crum WR, Hartkens T, Hill DLG (2004) Non-rigid image registration: theory and practice. Br J Radiol 77(Spec No 2):S140–S153

19. Nakamoto M, Nakada K, Sato Y, Konishi K, Hashizume M, Tamura S (2008) Intraoperative magnetic tracker calibration using a magneto-optic hybrid tracker for 3-D ultrasound-based navigation in laparoscopic surgery. IEEE Trans Med Imaging 27:255–270. doi:10.1109/TMI.2007.911003

20. Khan MF, Dogan S, Maataoui A, Wesarg S, Gurung J, Ackermann H, Schiemann M, Wimmer-Greinecker G, Vogl TJ (2006) Navigation-based needle puncture of a cadaver using a hybrid tracking navigational system. Invest Radiol 41:713–720. doi:10.1097/01.rli.0000236910.75905.cc

21. Feuerstein M, Reichl T, Vogel J, Traub J, Navab N (2009) Magneto-optical tracking of flexible laparoscopic ultrasound: model-based online detection and correction of magnetic tracking errors. IEEE Trans Med Imaging 28:951–967. doi:10.1109/TMI.2008.2008954

22. Markert M, Koschany A, Lueth T (2010) Tracking of the liver for navigation in open surgery. Int J Comput Assist Radiol Surg 5:229–235. doi:10.1007/s11548-009-0395-x

23. Nakamoto M, Ukimura O, Gill IS, Mahadevan A, Miki T, Hashizume M, Sato Y (2008) Realtime organ tracking for endoscopic augmented reality visualization using miniature wireless magnetic tracker. In: Proceedings of the 4th international workshop on medical imaging and augmented reality. Springer, Berlin, Heidelberg, pp 359–366

24. Maier-Hein L, Tekbas A, Seitel A, Pianka F, Müller SA, Satzl S, Schawo S, Radeleff B, Tetzlaff R, Franz AM, Müller-Stich BP, Wolf I, Kauczor H-U, Schmied BM, Meinzer H-P (2008) In vivo accuracy assessment of a needle-based navigation system for CT-guided radiofrequency ablation of the liver. Med Phys 35:5385–5396

25. Beller S, Eulenstein S, Lange T, Hünerbein M, Schlag PM (2009) Upgrade of an optical navigation system with a permanent electromagnetic position control: a first step towards "navigated control" for liver surgery. J Hepatobiliary Pancreat Surg 16:165–170. doi:10.1007/s00534-008-0040-z

26. Rassweiler JJ, Müller M, Fangerau M, Klein J, Goezen AS, Pereira P, Meinzer H-P, Teber D (2012) iPad-assisted percutaneous access to the kidney using marker-based navigation: initial clinical experience. Eur Urol 61:628–631. doi:10.1016/j.eururo.2011.12.024

27. Heald R, Ryall RD (1986) Recurrence and survival after total mesorectal excision for rectal cancer. The Lancet 327:1479–1482. doi:10.1016/S0140-6736(86)91510-2

28. Shekhar R, Dandekar O, Bhat V, Philip M, Lei P, Godinez C, Sutton E, George I, Kavic S, Mezrich R, Park A (2010) Live augmented reality: a new visualization method for laparoscopic surgery using continuous volumetric computed tomography. Surg Endosc 24:1976–1985. doi:10.1007/s00464-010-0890-8

29. Nickel F, Kenngott HG, Neuhaus J, Sommer CM, Gehrig T, Kolb A, Gondan M, Radeleff BA, Schaible A, Meinzer H-P, Gutt CN, Müller-Stich B-P (2013) Navigation system for minimally invasive esophagectomy: experimental study in a porcine model. Surg Endosc 27:3663–3670. doi:10.1007/s00464-013-2941-4

30. Maier-Hein L, Franz AM, Birkfellner W, Hummel J, Gergel I, Wegner I, Meinzer H-P (2012) Standardized assessment of new electromagnetic field generators in an interventional radiology setting. Med Phys 39:3424–3434. doi:10.1118/1.4712222